11–23% Cr steels for solid oxide fuel cell interconnect applications at 800 °C – How the coating determines oxidation kinetics

Available online at www.sciencedirect.com

ScienceDirect

journal homepage: www.elsevier.com/locate/he

11–23% Cr steels for solid oxide fuel cell interconnect applications at 800 °C – How the coating determines oxidation kinetics

M.J. Reddy [a,*], T.E. Chausson [b], J.E. Svensson [a], J. Froitzheim [a]

[a] Energy and Materials, Chalmers University of Technology Kemivägen 10, SE-41296 Gothenburg, Sweden
[b] INP-Ensiacet, 4, Allée Émile Monso - CS 44362 - 31030 Toulouse Cedex 4 - France

HIGHLIGHTS

- Uncoated ferritic steels have different chromium evaporation and oxidation rate.
- The steels show virtually identical, improved behaviour when coated with Ce/Co.
- The Ce/Co coatings reduced chromium evaporation by 60–100 times to uncoated.
- Ce/Co-coated AISI 409 (11.4 %Cr) didn't show breakaway corrosion after 3000 h.

GRAPHICAL ABSTRACT

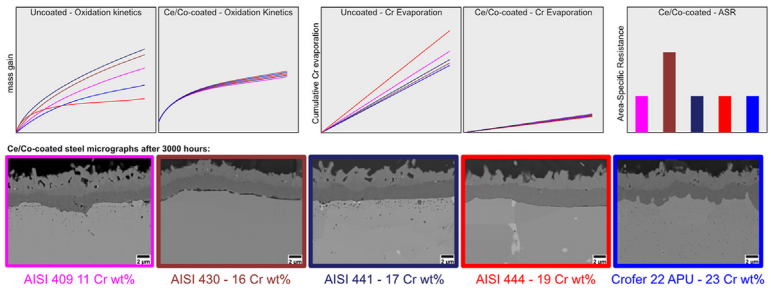

ARTICLE INFO

Article history:
Received 28 September 2022
Received in revised form
16 November 2022
Accepted 29 November 2022
Available online xxx

Keywords:
Solid oxide fuel cell
Ce/Co coating
Cr evaporation
Interconnect
Reactive element effect
Comparision

ABSTRACT

The present work investigates the low-cost steels AISI 441, AISI 430, and AISI 444 against the tailor-made high Cr steel Crofer 22 APU (22.9 wt% Cr) at 800 °C in simulated solid oxide fuel cell (SOFC) cathode conditions. Furthermore, a low Cr steel, AISI 409 (11.4 wt% Cr) is included in the study. The oxidation, chromium evaporation, and area-specific resistance (ASR) of the uncoated and Ce/Co-coated steels are studied for up to 3000 h. Ce/Co-coated steels showed significant improvement in behaviour compared to their uncoated counterparts. The oxidation and chromium evaporation behaviour between the uncoated steels varied substantially while the Ce/Co coated steels exhibited highly similar behaviour. The area-specific resistance of the coated low-cost steels was on par with Crofer 22 APU. However, 430 formed a continuous silica layer, resulting in a higher ASR after 3000 h. Cross-sections of the uncoated and Ce/Co-coated steels were analysed using a scanning electron microscope and energy dispersive X-ray spectroscopy.

* *Corresponding author.*
E-mail address: mareddy@chalmers.se (M.J. Reddy).

https://doi.org/10.1016/j.ijhydene.2022.11.326

Introduction

Solid Oxide Cells (SOC) are high temperature electrochemical cells that can convert fuel to electricity or electricity to fuel with very high efficiency. They are considered promising for decentralised electricity generation when operating in Solid Oxide Fuel Cell (SOFC) mode and hydrogen production when operating in Solid Oxide Electrolysis Cell (SOEC) mode. The interconnect is one of the critical components in a SOC stack, which plays the role of electrically connecting individual cells and acts as a physical barrier separating fuel and oxidant gases. Interconnect operates in demanding conditions with air and fuel atmospheres on either side. Therefore, the material selection for the interconnect application is stringent.

Progress in materials and manufacturing has led to a reduction in the working temperature of a SOC to the range of 600–900 °C, enabling metallic interconnects to replace traditional ceramics. Metallic materials usually have higher electrical and thermal conductivity, greater toughness, easier manufacturing, and lower cost than ceramics. Cr_2O_3-forming alloys exhibit good high temperature oxidation resistance and adequate oxide scale electrical conductivity; thus, they have been extensively investigated for use as SOC interconnects [1]. Among the Cr_2O_3-forming alloys, ferritic stainless steels (FSSs) are the most promising candidates because their thermal expansion coefficient is compatible with other SOC components (anode, cathode, and electrolyte), they are readily available, and have low manufacturing costs [2].

Nevertheless, FSSs have two significant issues: 1. chromia scale growth and 2. chromium evaporation. Chromia scale growth during exposure leads to increased electrical resistance across the cell, reducing cell efficiency. Furthermore, the chromia scale reacts with air in the presence of water vapour to form volatile chromium species Cr (VI) such as $CrO_2(OH)_2$. These volatile chromium species react with the cathode and are deposited at triple-phase boundaries, blocking the oxygen reduction reaction, which is known as cathode poisoning [3]. Cathode poisoning is an important degradation mechanism in SOFCs. Moreover, oxidation and chromium evaporation may lead to the depletion of Cr in the steel, resulting in the eventual breakdown of the protective scale.

Specialised steels, such as Crofer 22APU, Crofer 22H, and ZMG 232, have been developed to meet the challenging and, in part contradictory, material selection criteria for interconnects. These steels contain a large Cr reservoir for long-term operation, minor Mn additions to form an outer $(Cr,Mn)_3O_4$ spinel to mitigate chromium evaporation [4], and reactive elements (RE) to improve oxidation resistance and scale adherence [5]. The low-volume production and, in some cases, very low Si and Al content required in specifications make these tailor-made steels expensive.

Sachitanand et al. [6] have studied the oxidation and chromium evaporation properties of these steels. Despite advances made in adapting steel chemistry, these steels still have very high chromium evaporation and chromia growth; thus, they are not suitable for the long life expected for an interconnect. Hence, these steels must be appropriately coated with protective coatings to suppress chromium evaporation. Co and Mn-based spinel coatings (MCO) have been extensively researched for this application [7–12]. Furthermore, reactive elements in the coatings are known to have a beneficial effect on the oxidation performance of steel. Several researchers have shown that the RE in coatings significantly suppresses the chromia scale growth [13–15].

Different thin film coating technologies that include physical vapour deposition (PVD) [10,16,17], sol-gel dip coating [18], screen printing [19], electrophoretic deposition [20–22], and atmospheric plasma spray [23–25] are employed to deposit these coatings. Co and Mn-based spinel coatings can be formed by depositing metallic Co, which upon oxidation transforms into $(Co,Mn)_3O_4$ due to the outward diffusion of Mn from the steel [12,14]. These coatings are particularly suitable because they can be efficiently applied in a roll-to-roll, high-volume process [26]. Additionally, the self-healing properties of the metallic PVD coatings allow steel sheets to be shaped into an interconnect after coating [27]. Ce/Co coating with a 10 nm thick Ce layer beneath a 640 nm thick metallic Co layer has been extensively studied for the interconnect application [9,11,14,27–29].

The above studies show that a coating is inevitable for the application of FSS as interconnects. Other studies have indicated the possibility of using coated type 441 [9,11,24,29–31], 444 [32–36], and 430 [17,20,30,36–39] for an interconnect application. Goebel et al. [11] have shown that a Ce/Co-coated AISI 441 steel is stable for up to 38 000 h in air at 800 °C. Nevertheless, some challenges of using low-cost steels as interconnects include the formation of insulating SiO_2 scales, poor scale adherence, and lower oxidation resistance than the tailored steels. SiO_2 scales are perceived to be detrimental to SOFC performance due to high resistivity [2].

Some studies compared different bare substrates for their application as interconnect [6,36]. As the protective coating is inevitable, it is crucial to compare coated low-cost steels to tailor-made steels for their application as interconnect. Very few studies, however, have compared coated steels for their application as interconnects [30]. This study evaluates the oxidation, chromium evaporation, and ASR of Ce/Co-coated and uncoated Crofer 22 APU, AISI 444, AISI 441, AISI 430, and AISI 409 in typical SOFC conditions. Time-resolved mass gains, chromium evaporation, and ASR were measured at 800 °C, and the oxide scale was further characterised with SEM/EDX.

Experimental

Five chromia-forming FSS, AISI 409, AISI 430, AISI 441, AISI 444, and Crofer 22 APU were selected for this study. The thickness of AISI 409, and AISI 430 was 0.38 mm, while the thickness of AISI 441, AISI 444, and Crofer 22 APU was 0.3 mm. The materials are further referred to with their respective AISI number (eg. 441 instead of AISI 441). The compositions of the steels in weight% are shown in Table 1. A Ce/Co coating with 10 nm of Ce and 600 nm of Co (<1% Ce) was deposited on the steels using a proprietary PVD technique at Sandvik Materials Technology AB [26]. Coatings were deposited on pre-cut steel sheets with a coupon size of 15 * 17 mm. These coupons were cleaned using acetone and ethanol in an ultrasonic bath.

Please cite this article as: Reddy MJ et al., 11–23% Cr steels for solid oxide fuel cell interconnect applications at 800 °C – How the coating determines oxidation kinetics, International Journal of Hydrogen Energy, https://doi.org/10.1016/j.ijhydene.2022.11.326

Since the coating was deposited on pre-cut coupons, the edges of the coupons were also coated despite that PVD is a line-of-sight process. Reddy et al. [40] have found that the uncoated edges significantly influence the chromium evaporation measurements on the coated coupons.

The exposures were performed at 800 °C in a tubular furnace (Entech AB) in an air atmosphere containing 3% H_2O with a flow rate of 6000 sml min^{-1}.3% H_2O in the air was achieved by bubbling air through a heated water bath with a temperature >28 °C. The humidified gas subsequently passed a coil condenser maintained at 24.4 °C. The humidity was checked using a Michell Instruments Optidew Vision™ chilled mirror humidity sensor. A flow restrictor was used to minimize convection and ensure a uniform flow pattern in the reactor. Three coupons were used for each exposure in the reactor. Two types of exposures were performed: discontinuous isothermal mass gain measurements and continuous chromium evaporation measurements. The coupons in the mass gain exposures were periodically cooled to room temperature to follow mass gain over time measured using a Mettler Toledo XP6 scale before reheating. The time-resolved chromium evaporation behaviour of the coupons was investigated using the denuder technique, allowing in-situ determination of chromium evaporation. A Na_2CO_3 coated denuder tube was placed at the outlet of the reactor to collect Cr (VI) species. The coated denuder tube was replaced at regular intervals without affecting the exposure. A detailed description of the measurement procedure is given elsewhere [41]. Chromium evaporation exposures were performed on uncoated and coated coupons for 500 h and 1000 h, respectively. After chromium evaporation, the mass gain was measured, and minimal difference in mass gain is observed from the discontinuous exposures (mass gain exposures).

Area-specific resistance measurements were carried out ex-situ on the coated coupons exposed for 3000 h. A thin layer of platinum was sputtered on top of the oxide scale after exposure using a sputter coater. After sputtering, a platinum paste (Metalor 6926) was applied to the sputtered area. These coupons were further dried at 150 °C for 10 min followed by a sintering step at 800 °C for 1 h. The resistance was conducted at 800 °C using a 4-point mode. A Keithley 2400 source metre was used for the measurement with the applied current set at 100 mA/cm^2. Semiconductor behaviour was checked by monitoring the ASR as the coupons cooled. A more detailed description of ASR measurements is found elsewere [9].

After the exposure, cross-sections of coated coupons were prepared using a Leica EM TIC 3X Broad Ion Beam (BIB) milling system. The microstructure and chemical composition of the oxide scale was analysed using a JEOL JSM-7800F Prime SEM equipped with an Oxford Instruments Energy-Dispersive X-ray spectrometer (EDX).

Results

Fig. 1a and b shows the cumulative chromium evaporation and the rate of chromium evaporation of the uncoated steels Crofer 22 APU, 444, 441, 430, and 409 exposed at 800 °C. The uncoated steels exhibited dissimilar cumulative chromium evaporation. 430, 441 and Crofer 22 APU had significantly lower cumulative chromium evaporation than 444. Crofer 22 APU had the lowest cumulative chromium evaporation of the investigated materials. All the uncoated coupons showed a reduction in the rate of chromium evaporation as a function of time except for 409. Crofer 22 APU, 430, and 441 showed a significant decrease in chromium evaporation rate during the first week, followed by a steady-state rate. In contrast, 444 took much longer to attain the steady-state rate, which caused the higher cumulative chromium evaporation shown in Fig. 1a. Nevertheless, 441 and 444 had a similar rate of chromium evaporation, while 430, Crofer 22 APU was slightly lower after 500 h. Uncoated 409 had the highest rate of chromium evaporation after 500 h. Moreover, the chromium evaporation of uncoated 409 increased as opposed to other steels, which showed a gradual decrease with time. This is attributed to severe spalling of the oxide scale observed on the steel only after 168 h.

Fig. 2a and b shows the cumulative chromium evaporation and the rate of chromium evaporation of Ce/Co-coated Crofer 22 APU, 444, 441, 430, and 409 exposed at 800 °C for 1000 h in the air with 3% H_2O. The cumulative chromium evaporation of the coated coupons was extremely low. All the Ce/Co-coated substrates showed similar cumulative chromium evaporation after 500 h and the rate of chromium evaporation was similar regardless of the behaviour of the uncoated material. The rate of chromium evaporation of the coated coupons remained constant throughout the exposure in contrast to the uncoated steels. Ce/Co-coated steels have previously been reported to reduce chromium evaporation by one order of magnitude compared to uncoated steels [12,29,42–45]. The coated coupons used in these studies were cut from a coated steel sheet and thus had uncoated edges. More detailed information on the influence of uncoated edges on coated coupons can be found here [40]. Ce/Co coatings on Crofer 22 APU, 444, 441, 430, and 409 in the present study reduced the chromium evaporation by about 60–100 times compared to the respective uncoated steels at 800 °C. The reduction in chromium evaporation achieved with Ce/Co coatings was much

Table 1 – Chemical composition of the selected alloys in weight %.

Alloy	Fe	Cr	C	Mn	Si	Ti	Nb	Mo	La
Crofer 22 APU (1.4760)	Bal	22.92	0.004	0.38	0.01	0.06			0.07
AISI 444 (1.4521)	Bal	19.03	0.015	0.35	0.40	0.005	0.6	1.86	
AISI 441 (1.4509)	Bal	17.56	0.014	0.35	0.59	0.17	0.39		
AISI 430 (1.4016)	Bal	16.2	0.04	0.49	0.34				
AISI 409 (1.4512)	Bal	11.4	0.012	0.39	0.51	0.17			

Please cite this article as: Reddy MJ et al., 11–23% Cr steels for solid oxide fuel cell interconnect applications at 800 °C – How the coating determines oxidation kinetics, International Journal of Hydrogen Energy, https://doi.org/10.1016/j.ijhydene.2022.11.326

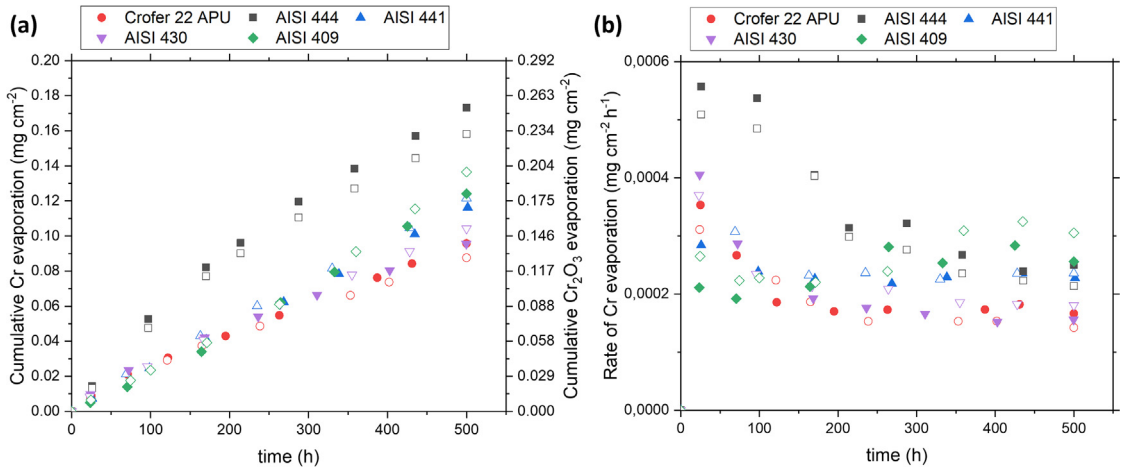

Fig. 1 – (a) Cumulative chromium evaporation (b) rate of chromium evaporation as function of time of the uncoated steels exposed to 800 °C in air + 3% H_2O for 500 h isothermally. Open and filled symbols represent two individual exposures.

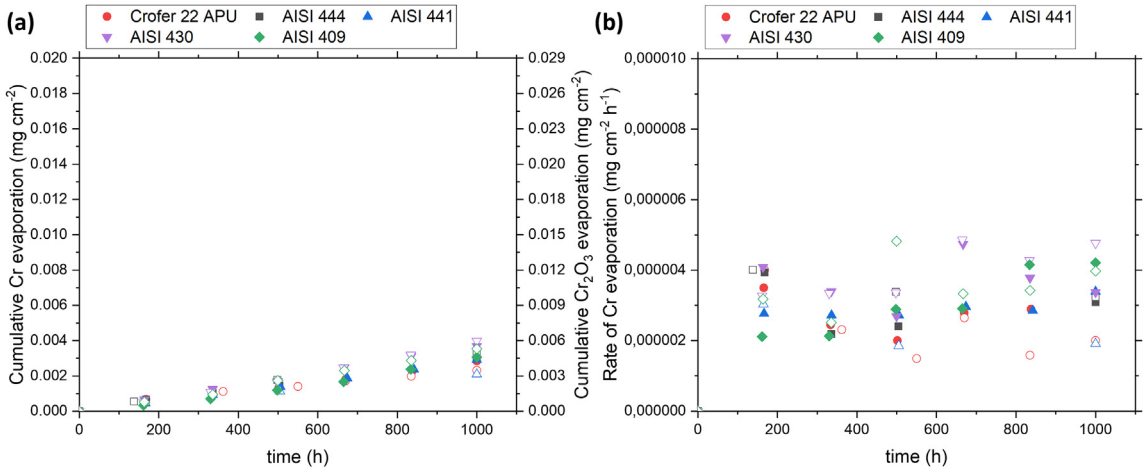

Fig. 2 – (a) Cumulative chromium evaporation (b) rate of chromium evaporation as a function of time for the Ce/Co-coated steels exposed to 800 °C in air + 3% H_2O for 1000 h isothermally. Open and filled symbols represent two individual exposures.

greater for 444 and 409, as they had much higher chromium evaporation when uncoated.

Fig. 3a shows the net mass gain of the uncoated steels Crofer 22 APU, 444, 441, 430, and 409 exposed at 800 °C for 500 h in the air with 3% H_2O. Net mass gain i.e., the gravimetrically measured mass gain is the sum of mass gain due to oxidation and mass loss due to chromium evaporation. Each point is an average of at least six coupons, while the error bars represent standard deviation. The uncoated steels showed an increase in net mass with time. None of the steels showed signs of spallation except 409 which had spallation already after 168 h into the exposure. 444 had a rapid net mass gain during the first 168 h but exhibited a slow mass gain later on till 500 h. On the other hand, 409, 430, 441, and Crofer 22 APU had a slower but continuous net mass gain with time. The difference in the net mass gain between the selected steels increased over time. After 500 h, 444 had the least mass gain, followed by Crofer 22 APU, 430, 409, and 441. These findings agree well with earlier published data on 444, showing that 444 has a slower rate of oxide scale growth than 441 at 750 °C and 850 °C [46]. The mass gains measured after chromium evaporation (isothermal exposure) for 500 h are similar to the mass gains measured during the discontinuous exposure except for 409. This is likely due to the excessive spallation observed on 409.

Fig. 4 shows the broad ion beam milled cross-section of the uncoated steels exposed for 500 h at 800 °C in air with 3% H_2O. The micrographs reveal that the oxide scale was intact after 500 h except for 409. Fig. 5 shows EDX maps of the cross-sections of the uncoated steels exposed for 500 h at 800 °C. The oxide scale structure was similar for all the uncoated steels with a $(Cr,Mn)_3O_4$ spinel on the top and a Cr_2O_3 layer beneath it. Despite the excessive spallation on 409, no iron-rich non-protective oxides were observed on 409, indicating a protective layer. The steels 441 and 444 showed laves phase precipitates in the matrix. A higher fraction of laves phase precipitates was found in 444 than in 441. No laves phase precipitates were found for 409, 430, and Crofer 22 APU, as

Please cite this article as: Reddy MJ et al., 11–23% Cr steels for solid oxide fuel cell interconnect applications at 800 °C – How the coating determines oxidation kinetics, International Journal of Hydrogen Energy, https://doi.org/10.1016/j.ijhydene.2022.11.326

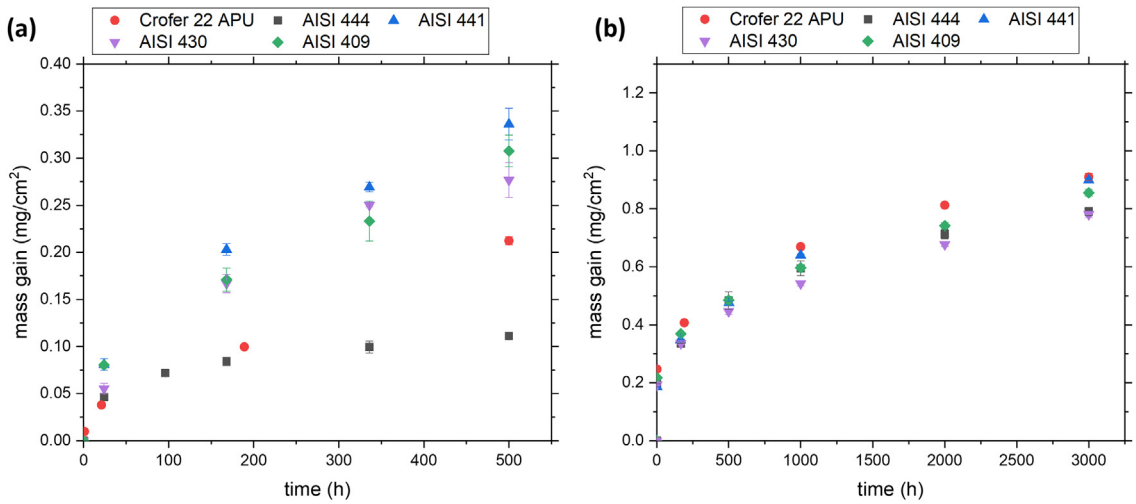

Fig. 3 – Net mass gain as a function of time for (a) uncoated steels exposed for 500 h and (b) Ce/Co-coated steels exposed at 800 °C in air + 3% H_2O. Error bars represent standard deviation.

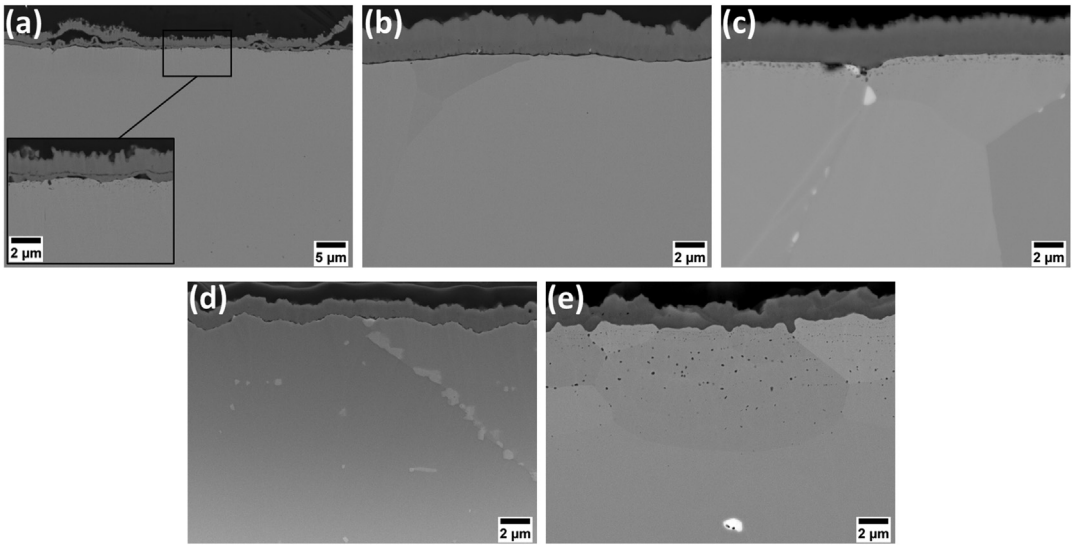

Fig. 4 – BIB milled cross-sections of the uncoated steels (a) AISI 409, (b) AISI 430, (c) AISI 441 (d) AISI 444, and (e) Crofer 22 APU exposed for 500 h at 800 °C in air + 3% H_2O.

expected. The chromia scale thicknesses were different on the steels after 500 h, which agrees well with the observed net mass gains.

Fig. 3b shows the net mass gain for the Ce/Co-coated steels Crofer 22 APU, 444, 441, 430, and 409 exposed at 800 °C for 3000 h in air with 3% H_2O. The coated steels showed a rapid mass gain during the first 2 h. This was attributed to the oxidation of the 600 nm metallic Co in the coating to Co_3O_4, which corresponds to a theoretical mass gain of 0.21 mg/cm^2, as reported previously [14,29]. After the initial 2 h, all the coated steels showed a continuous increase in mass with time, following parabolic oxidation kinetics as shown in Figure A1 in the supplemental material. The mass gain was not significantly influenced by chromium evaporation due to the extremely low chromium evaporation from the coated coupons. It is noteworthy that all the coated steels had very similar mass gains despite the differences in the mass gains of the uncoated steels. 409 with only 11.4 wt% Cr in the matrix, which showed excessive spallation only after 168 h when uncoated, did not show any signs of breakaway within 3000 h when coated with Ce/Co.

Fig. 6 shows the broad ion beam milled cross-section of the Ce/Co-coated steels exposed for 3000 h at 800 °C in air with 3% H_2O. The micrographs reveal that the coatings and the oxide scale of all samples were intact after 3000 h. The oxide scale structure was similar for all the Ce/Co-coated steels with an oxidized coating on top and a chromia layer beneath it. The chromia scale thicknesses were very similar after 3000 h, which agrees well with the observed similarity in net mass gains. The chromia scale on Crofer 22 APU is more undulating than on the other steels. Fig. 7 shows the EDX maps of the cross-sections of the Ce/Co-coated steels exposed for 3000 h at

Please cite this article as: Reddy MJ et al., 11–23% Cr steels for solid oxide fuel cell interconnect applications at 800 °C – How the coating determines oxidation kinetics, International Journal of Hydrogen Energy, https://doi.org/10.1016/j.ijhydene.2022.11.326

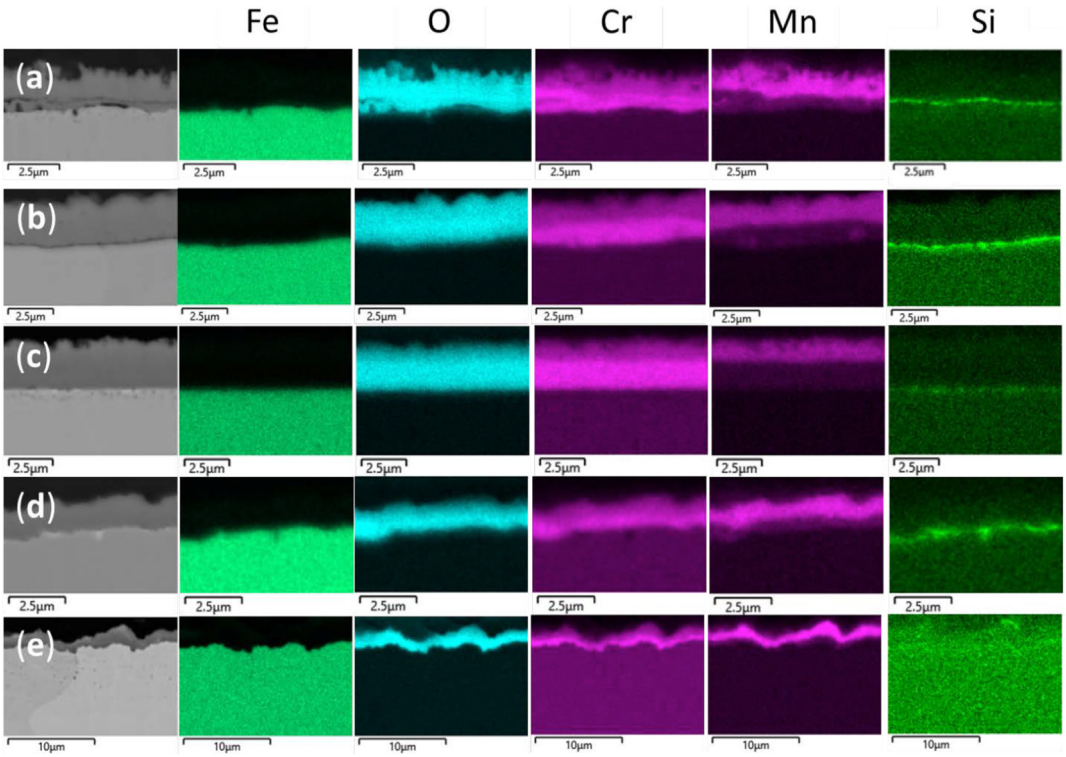

Fig. 5 – EDX maps of the BIB milled cross-sections of the uncoated steels (a) AISI 409, (b) AISI 430, and (c) AISI 441 (d) AISI 444 (e) Crofer 22 APU exposed for 500 h at 800 °C in air + 3% H_2O.

800 °C. The EDX maps indicate that all the Ce/Co-coated steels had a multi-layered oxide scale structure. The outer scale was rich in Co, Mn, with some Fe. Below the outer scale, a continuous chromia scale is visible on all the coated steels in Fig. 7. One significant difference is observed in the Si map. The low-cost steels, 441, 444, 430, and 409, had a Si-rich scale formation at the metal-oxide interface. Such a scale was not observed in Crofer 22 APU as a consequence of the lower Si content in the alloy.

Fig. 8 shows the ASR of the Ce/Co-coated steels exposed for 3000 h at 800 °C. The ASR of the Ce/Co-coated steels 409, 441, 444, and Crofer 22 APU ranged from 18 to 23 mohm cm^{-2} when measured after 3000 h at 800 °C. The oxide scale showed semiconducting behaviour with increased electrical

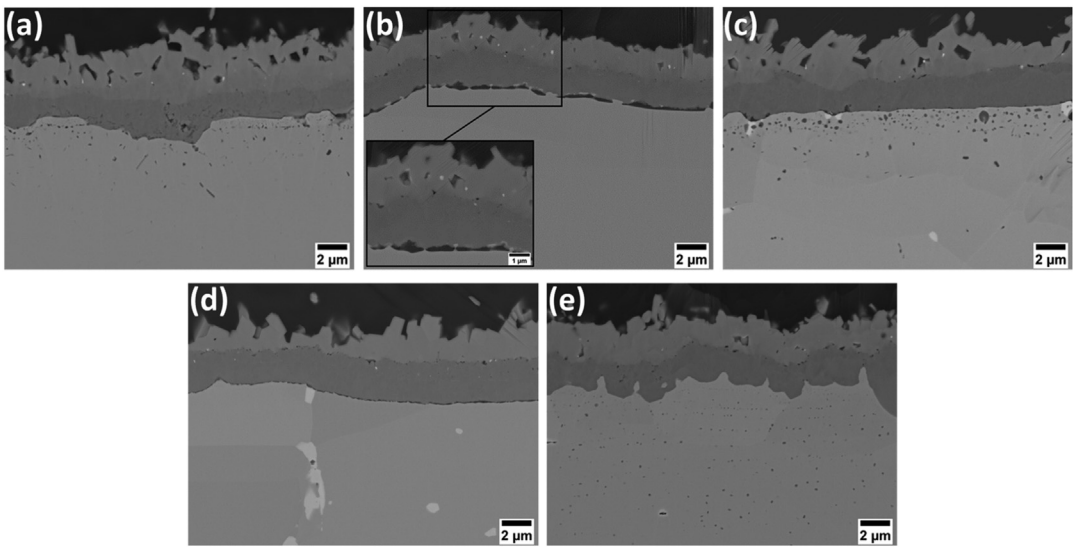

Fig. 6 – BIB milled cross-sections of the Ce/Co-coated steels (a) AISI 409, (b) AISI 430, and (c) AISI 441 (d) AISI 444 (e) Crofer 22 APU exposed for 500 h at 800 °C in air + 3% H_2O.

Please cite this article as: Reddy MJ et al., 11–23% Cr steels for solid oxide fuel cell interconnect applications at 800 °C – How the coating determines oxidation kinetics, International Journal of Hydrogen Energy, https://doi.org/10.1016/j.ijhydene.2022.11.326

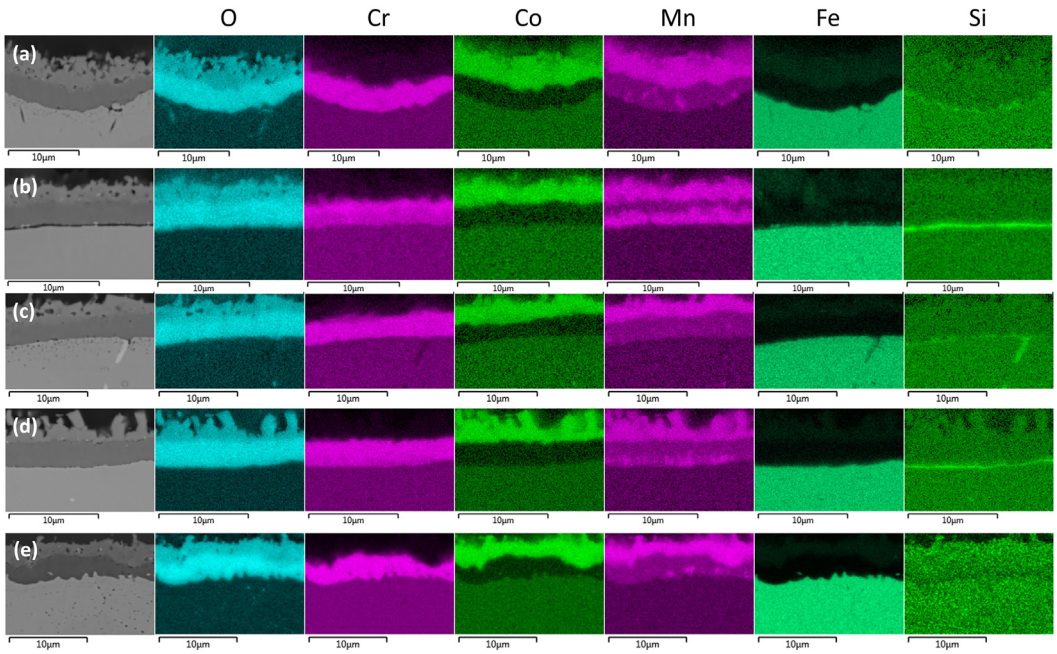

Fig. 7 – EDX maps of the BIB milled cross-sections of the Ce/Co-coated steels (a) AISI 409, (b) AISI 430, and (c) AISI 441 (d) AISI 444 (e) Crofer 22 APU exposed for 3000 h at 800 °C in air + 3% H_2O.

resistance as the temperature decreased. However, 430 showed a high ASR after 3000 h in the range of 45 mohmcm^2.

Discussion

Chromium evaporation

Although the uncoated steels showed a difference in cumulative chromium evaporation, this difference was mostly due to variations in the initial rate of chromium evaporation. The rate of chromium evaporation after 500 h was similar for 441 and 444, and it was slightly lower for Crofer 22 APU and 430.

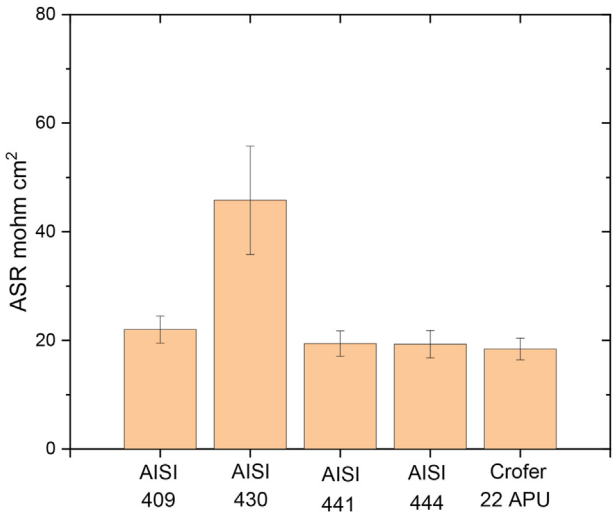

Fig. 8 – Ex-situ area-specific resistance measured with a current of 100 mA on the Ce/Co-coated steels exposed for 3000 h at 800 °C in air +3% H_2O.

The decrease in the rate of chromium evaporation was because of the incorporation of Mn into the oxide layer. Mn diffusion to the surface results in the formation of $(Cr,Mn)_3O_4$, which is known to reduce chromium evaporation by 2–3 times at 800 °C compared to Cr_2O_3 [4,47]. Despite that all the steels had similar Mn content, 444 took much longer to reach a similar rate of chromium evaporation as 441. This may be attributable to the slower diffusion of Mn to the surface of Mo-containing steel due to the higher fraction of laves phases in the bulk and along the grain boundaries. Since Crofer 22 APU and 430, have no laves phases, the chromium evaporation decreased faster and have a lower rate of chromium evaporation after 500 h.

The combined presence of Mo and Nb results in higher laves phase precipitation than in Nb-containing steels such as 441 [48]. Higher laves phase precipitation might affect the diffusion of Mn to the oxide scale. Ali-Löytty et al. [48] have shown that $(FeCrSi)_2(MoNb)$ laves phases formed at grain boundaries strongly limit the diffusion of Mn to the oxide scale at 650 °C. The initially higher rate of chromium evaporation of Mo-containing steels has been reported earlier, which supports this hypothesis: the initial rate of chromium evaporation of 444 is higher than 441 [46], and Sanergy HT is higher than Crofer 22H [49] at 750 °C. No difference in chromium evaporation between 441 and 444, having similar Mn concentrations, was found at 850 °C [46,50]. This finding is attributed to the faster formation of a $(Cr,Mn)_3O_4$ spinel at higher temperatures possibly in combination with a larger share of bulk Mn diffusion to the surface, which would minimize the effect of the laves phases on Mn diffusion.

Chromium evaporation increases the consumption of Cr in steel and thus accelerates the depletion of the Cr reservoir in an alloy. This might result in breakaway oxidation and rapid oxidation due to the formation of less protective oxide scales,

Please cite this article as: Reddy MJ et al., 11–23% Cr steels for solid oxide fuel cell interconnect applications at 800 °C – How the coating determines oxidation kinetics, International Journal of Hydrogen Energy, https://doi.org/10.1016/j.ijhydene.2022.11.326

such as iron oxides. Based on the chromium evaporation data, it can be concluded that none of the selected steels are suitable for interconnect applications without protective coatings for the estimated 80000 h of service life for interconnects.

The Ce/Co coatings reduced the chromium evaporation of the steels by 60–100 times, forming a $(Co,Mn)_3O_4$ spinel on a chromia scale. The Co coating transforms to $(Co,Mn)_3O_4$ spinel due to the diffusion of Mn from steel to the coating [12,51,52]. This data agrees with earlier reported data on the efficiency of $(Co,Mn)_3O_4$ spinel in reducing chromium evaporation [4,7,53–55]. The cumulative chromium evaporation of coated 444 was almost 100 times lower than the uncoated 444 after 500 h. Such a high reduction in chromium evaporation on a Ce/Co-coated 444 was due to the higher chromium evaporation of the uncoated 444. Metallic Ce/Co coatings form a cap layer of Co_3O_4 upon exposure. Over time this layer becomes enriched in Mn and Fe. Thus, Cr evaporation is effectively blocked, and the efficiency of the layer doesn't rely on Mn diffusion. For this reason, all coated materials showed similar chromium evaporation data irrespective of the slower diffusion of Mn to the coating in the case of 444. Hence, the development of steel coating combinations should focus on oxidation and electrical properties.

Corrected mass gains

The oxidation of a metal specimen is usually determined in terms of mass gain due to the pickup of oxygen. Mass gain data are used to understand and predict the oxidation behaviour of steel. However, chromium evaporation results in a loss of oxide scale and thus affects mass gain, too. The measured mass gain in Fig. 3 is termed net mass gain. The measured mass gain when corrected for chromium lost through evaporation is termed as corrected or gross mass gain.

Table 2 shows the net mass gains and corrected mass gains of uncoated 430, 441, 444, and Crofer 22 APU after 500 h. Due to excessive spallation and dissimilar mass gains in isothermal and discontinuous measurements, the corrected mass gains of 409 are not shown. The net mass gain (gravimetrically measured) is the sum of mass gain due to oxidation and mass loss due to chromium evaporation. Net mass gain gives an inaccurate measure of the extent of oxidation and Cr consumption in an alloy. The corrected mass gain (calculated from chromium evaporation and net mass gain data), corresponds to the total oxide scale formed on the surface of the steel. The Cr surface from the steel is lost as Cr_2O_3. It was calculated that 1 mg of Cr collected equals 1.46 mg of Cr_2O_3 lost from the oxide scale [6,50]. For coated samples, the net- and gross mass gain are virtually identical due to the low chromium evaporation.

Table 2 – Net mass gains and corrected mass gains of uncoated 430, 441, 444, and Crofer 22 APU after 500 h.

Steel	Net mass gain (mg/cm^2)	Gross mass gain (mg/cm^2)
AISI 430	0.27	0.42
AISI 441	0.33	0.50
AISI 444	0.11	0.34
Crofer 22 APU	0.21	0.34

Oxidation behaviour – uncoated steels

444 showed the lowest net mass gain of the selected steels after 500 h, roughly half of the Crofer 22 APU net mass gain. Nevertheless, the Cr consumption of 444, as depicted by the corrected mass gains, was similar to that for Crofer 22 APU after 500 h. Conversely, 430, 441, and Crofer 22 APU showed significant differences in net and corrected mass gains despite having equivalent chromium evaporation. This is expected to be due to the presence of La in Crofer 22 APU, which is known to improve the oxidation resistance of Cr_2O_3 forming alloys [5]. The corrected mass gain of 444 was still lower than that for 430 and 441 despite that it had higher chromium evaporation and no reactive elements. The results are in agreement with earlier studies on uncoated 441 and 444 [46,50,56,57]. The beneficial effect of reactive elements has been known for decades although the exact mechanism is still debated. The most widely accepted explanation is that undoped Cr_2O_3 grows primarily by outward diffusion of Cr^{+3} with a secondary contribution by inward diffusion of O^{-2}. In contrast, in RE doped Cr_2O_3, REs block the outward diffusion of Cr^{+3} ions [58]. Hence the overall growth rate is drastically reduced and the chromia growth direction changes from primarily outward to inward growth. A detailed discussion of the RE effect can be found in Refs. [59–61].

Influence of steel composition

The significant differences observed in the oxidation and chromium evaporation of the uncoated steels are related to their chemical composition, given in Table 1. The presence of a reactive element, La, in Crofer 22 APU is known to improve the oxidation resistance [5,62]. Although the details of the reactive element effect mechanism are still debated, minor additions of reactive elements are known to enhance the oxidation resistance, reduce spallation by improving oxide scale adhesion, and modify the microstructure oxide scale. Uncoated 409 showed excessive spallation, however, once coated with a reactive element containing coating (Ce), no spallation is observed even after 3000 h.

The presence of Ti in Crofer 22 APU, 409, and 441 might increase the oxidation rate of these alloys. Ti is reported to increase the oxidation rate of the steel by doping the chromia scale. Ti^{+4} doping results in the creation of chromium vacancies, which increases the diffusion rate of Cr^{+3}, resulting in an increased oxidation rate [63,64]. A similar mechanism is postulated for Nb doping of chromia scale, which is present in 441 and 444 [65].

The differences in the Si maps at the metal-oxide interface in the EDX analysis as seen in Figs. 5 and 7 can be explained by the chemical composition of the steels. Silicon is often a remnant of the steel-making process where it is used as a deoxidiser. The Si content in Crofer 22 APU is much lower compared to the low-cost steels, 430, 441, and 444. This is due to the vacuum melting process undergone by Crofer 22 APU, which adds cost to the manufacturing process. The Si in the

Please cite this article as: Reddy MJ et al., 11–23% Cr steels for solid oxide fuel cell interconnect applications at 800 °C – How the coating determines oxidation kinetics, International Journal of Hydrogen Energy, https://doi.org/10.1016/j.ijhydene.2022.11.326

steel matrix diffuses to the metal-oxide interface over time and oxidized to SiO_2.

The presence of Nb in 441 and 444 leads to the formation of laves phases, a Fe_2Nb based intermetallic phase with a C14 hexagonal crystal structure [31]. The precipitation of laves phases is also enhanced by Ti in 441 [31] and Mo in 444 [66]. The volume of laves phase precipitates is higher for 444 than for 441. It is speculated that a higher amount of laves phases in 444 leads to low oxidation as observed in Fig. 7 [56]. Laves phases are known to bind Si, reducing the free Si in the matrix, resulting in a thinner silica scale at the metal-oxide interface [67]. Nevertheless, the formation of SiO_2 cannot be entirely avoided by optimising the ratio between Si and Nb [31]. Hence, the Si maps in Fig. 5 show the silica layer formed at the metal-oxide interface. The EDX maps in Figs. 5 and 7 show more prominent SiO_2 at the metal-oxide interface in 444 despite that 444 has a lower Si content and a higher fraction of laves phases than 441. The reasons for this are not clearly understood. 430 which does not contain Ti, Mo, and Nb showed a prominent Si scale formation at the metal-oxide interface. The point analysis in Figure A2 (appendix) shows that up to 10 atomic % of Si is found at the metal-oxide interface.

Oxidation behaviour – coated steels

The mass gain data of Ce/Co-coated steels in Fig. 4 shows that there is no difference in the mass gains of the coated steels after 3000 h, in contrast to the uncoated steels. This is surprising considering the variation in mass gain behaviour of the uncoated steels. These results agree with earlier published results showing that Co/CeO_2 coated Crofer 22 APU and Crofer 22H have similar mass gains [51]. However, the results do not confirm the previous research by Talic et al. [30], where differences in the oxidation rates of $MnCo_2O_4$ coated steels 430, 441, and Crofer 22H at 650, 700, and 750 °C were observed. Such differences can be attributed to two reasons: Firstly, the $MnCo_2O_4$ coated steels had been sintered at 900 °C before exposure. The different oxide scales formed during sintering might have different thicknesses resulting in different oxidation kinetics. Secondly, the lack of reactive elements in the $MnCo_2O_4$ coating might result in different oxidation properties.

Froitzheim et al. [12] have shown that a thin Co coating without Ce does not improve the oxidation behaviour of Sanergy HT. Several authors have reported an improvement in the oxidation rate of Crofer 22 APU with reactive element coatings despite the alloy containing La [18,68–70]. Thus, a beneficial effect either due to a higher concentration of RE at the surface or a combined effect of different REs seems likely. Although the reactive element effect mechanism is not fully understood, the Ce/Co-coated steels seem to benefit from the same kind of RE doping resulting in highly similar oxide scales. Results show that increasing the doping of the Ce in the coating from 10 nm to 20 and 50 nm did not show any improvement in the oxidation behaviour up to 6000 h at 800 °C [71].

Cr reservoir

Chromium content in steel plays an important role in the design of alloys for the interconnect. The Cr content of 20 wt% or more was used in the steels designed for the interconnect application, in part to match thermal expansion but also to maintain long-term oxidation resistance at high operating temperatures. This was the idea behind the development of Crofer 22 APU, Crofer 22H, and Sanergy HT. Several authors [44,72] proposed that the interconnect will undergo breakaway corrosion once the Cr content in the steel falls below 15 wt%. However, in the present study, it is found that 409, with Cr 11.4 wt% lasted for 3000 h without breakaway corrosion. Similarly, Goebel et al. [11] have reported that the Cr content in bulk of Ce/Co-coated 441 exposed for 38 000 h is 12 wt% and breakaway corrosion is not observed.

Area-specific resistance

Besides reducing Cr evaporation several authors have established that coated steels have much lower ASR than uncoated steels [9,11,29,73]. The ASR data from the present work show that coated steels have highly similar ASR values except 430. This might be surprising considering the varying Si content in the steels. A SiO_2 layer formed at the metal-oxide interface is clearly visible on 409, 430, 441, and 444, as shown in the EDX maps in Fig. 5. Nevertheless, such SiO_2 subscale is not formed on Crofer 22 APU due to low Si content in the steel. The formation of a SiO_2 subscale has been reported to increase ASR and decrease SOFC performance. SiO_2 is highly resistive with a conductivity of 10^{-5} to 10^{-7} S. cm^{-1} at 800 °C [74]. It can be estimated that 10 nm of silica translates into an ASR of 100–10000 mΩ cm^2 for a 1 cm^2 contact area at 800 °C.

The ASR of the Ce/Co-coated steels measured after 3000 h depends on the oxide scales formed. It can be seen in the EDX maps in Fig. 5 that the scale has three types of layers: $(Co,Mn)_3O_4$; Cr_2O_3; and SiO_2. SiO_2 is not present in the case of Ce/Co-coated Crofer 22 APU. The three oxides are interpreted as in-series connected resistors. At 800 °C, the conductivity of $Co_xMn_{3-x}O_4$ varies from 6.4 to 60 S cm^{-1} [75] and Cr_2O_3 varies from 0.001 to 0.05 S cm^{-1} [76,77]. Table 3 shows the contribution of ASR by $Co_xMn_{3-x}O_4$, Cr_2O_3, and SiO_2. Due to the high conductivity of $Co_xMn_{3-x}O_4$ the contribution of the coating to ASR is negligible compared to the chromia scale. Moreover, all coated materials had a chromia scale with a similar thickness, which is expected to result in similar contributions to ASR. Based on the literature data, the calculated ASR for the coated steels varied from 4 to 200 mΩ cm^2 without considering the presence of a SiO_2 scale. This fits well with the measured ASR of 20 ± 3 mΩ cm^2 except for 430 which showed 50 ± 4 mΩ cm^2.

The predicted influence of the SiO_2 subscale on the measured ASR was not observed experimentally. However, these results agree with earlier published findings where several authors have found little effect of Si on ASR for up to 3000 h [78,79]. The reasons that the Si scale had little influence might be that either the Si-rich resistive oxide scale is not continuous, or the Si-rich resistive oxide is substantially more conductive than the literature value for SiO_2. However, 430 exhibits a substantially higher ASR. This is attributed to the Si-rich subscale as 430 does not have any laves phase that binds Si in the steel matrix, consequently, the Si layer is most pronounced in 430 (see Fig. 7 and Figure A2).

Please cite this article as: Reddy MJ et al., 11–23% Cr steels for solid oxide fuel cell interconnect applications at 800 °C – How the coating determines oxidation kinetics, International Journal of Hydrogen Energy, https://doi.org/10.1016/j.ijhydene.2022.11.326

Table 3 – ASR values calculated from the thickness of the $Co_xMn_{3-x}O_4$, Cr_2O_3 and SiO_2 layers.

Oxide	Average thickness	Conductivity (S cm^{-1})		ASR (mohm cm^2)	
		Min	Max	Min	Max
$Co_xMn_{3-x}O_4$ [75]	1 μm	6.4	60	0.001	0.015
Cr_2O_3 [76,77]	2 μm	0.001	0.05	4	200
SiO_2 [74]	10 nm	10^{-7}	10^{-5}	100	10 000

Possibilities and limitations of low-cost steels

409 has only 11.4 wt% Cr in the steel, which is extremely low and cannot be used as an interconnect for several 10 000 h. 430, 441, and 444 are low-cost steels and readily available in the market with at least 16 wt% Cr. The lack of reactive elements and high production volumes make these steels cheaper. However, the uncoated low-cost steels, 430, 441, and 444, performed worse than Crofer 22 APU with respect to chromium evaporation and/or oxidation. Nevertheless, it has been established that uncoated steels cannot be used for interconnect applications due to the high chromium evaporation and oxidation of these materials. The results of this work show that the performance of Ce/Co-coated steels alleviates these problems.

The differences between the five investigated materials in terms of chromium evaporation and oxidation were negligible once a Ce/Co coating had been applied. Particularly interesting is that no difference in ASR was found between the coated steels except for 430. Despite the long exposure duration of 3000 h, this represents only a small fraction of the required lifetime of interconnect. Based on the ASR data of Ce/Co 430, the effect of Si on the performance of the interconnect must not be ignored.

Moreover, SiO_2 can cause spallation in low-cost FSS due to the low CTE of SiO_2 [80,81]. Although no spallation was observed till 3000 h, adhesion of the oxide scale in the long term must be evaluated. The evolution of the SiO_2 subscale and its effect on long-term operation must be explored. 441 and 444 have a lower Cr reservoir than Crofer 22 APU. Since the Cr consumption behaviour of all the coated steels was identical as indicated by the mass gain measurements, material failure might occur first on low-cost steels when the Cr concentration falls below a certain level. Detailed consumption of Cr by the oxide layer in the long term must be evaluated.

Conclusion

The effect of Ce/Co coating on AISI 409, AISI 430, AISI 444, AISI 441, and Crofer 22 APU was investigated in air with 3% H_2O at 800 °C and compared with the uncoated steels. The steels exhibited different levels of chromium evaporation and chromia scale growth. Once coated with a Ce/Co coating, the performance of the steels was significantly better than that of the uncoated steels for the interconnect application. The coated steels exhibited highly similar levels of chromium evaporation, and the coatings reduced the chromium evaporation of the selected steels by at least 60 times at 800 °C compared to the uncoated ones. All the coated steels showed similar oxide scale structure and thickness. The ASR of the coated steels after 3000 h was similar, about 18–23 mΩ cm^2 except for AISI 430. The high ASR for AISI 430 is attributed to the formation of continuous SiO_2 subscale formation at the metal-oxide interface. Although a SiO_2 subscale was found at the metal-oxide interface of 409, 441, and 444, it did not significantly influence the ASR measurements of these steels. Low-cost steels appear to be as effective as tailor-made Crofer 22 APU in chromium evaporation, mass gain, and ASR at 800 °C for 3000 h.

Declaration of competing interest

The authors declare that they have no known competing financial interests or personal relationships that could have appeared to influence the work reported in this paper.

Acknowledgments

This work was performed within the Swedish High Temperature Corrosion Centre. This project has received funding from the Fuel Cells and Hydrogen 2 Joint Undertaking under Grant Agreement No 826323. This Joint Undertaking receives support from the European Union's Horizon 2020 Research and Innovation programme, Hydrogen Europe and Hydrogen Europe Research. This work was also supported by the strategic innovation program Metalliska Material (Vinnova grant 2021–01003) a joint program of VINNOVA, Formas and the Swedish Energy. This work was performed in part at the Chalmers Material Analysis Laboratory (CMAL).

Appendix A. Supplementary data

Supplementary data to this article can be found online at https://doi.org/10.1016/j.ijhydene.2022.11.326.

REFERENCES

[1] Chevalier S, et al. CHAPTER 6 development of SOFC interconnect stainless steels. Solid State Phenom 2020;300:135–56.

[2] Niewolak L, Tietz F, Quadakkers WJ. Interconnects. In high-temperature solid oxide fuel cells for the 21st century: fundamentals, design and applications. 2nd ed. Academic

Press; 2016. p. 195–254. https://doi.org/10.1016/B978-0-12-410453-2.00007-5.
[3] Jiang SP, Chen X. Chromium deposition and poisoning of cathodes of solid oxide fuel cells - a review. Int J Hydrogen Energy 2014;39:505–31.
[4] Stanislowski M, et al. Reduction of chromium vaporization from SOFC interconnectors by highly effective coatings. J Power Sources 2007;164:578–89.
[5] Hou PY, Stringer J. The effect of reactive element additions on the selective oxidation, growth and adhesion of chromia scales. Mater Sci Eng, A 1995;202:1–10.
[6] Sachitanand R, Sattari M, Svensson JE, Froitzheim J. Evaluation of the oxidation and Cr evaporation properties of selected FeCr alloys used as SOFC interconnects. Int J Hydrogen Energy 2013;38:15328–34.
[7] Talic B, et al. Effect of coating density on oxidation resistance and Cr vaporization from solid oxide fuel cell interconnects. J Power Sources 2017;354:57–67.
[8] Talic B, Hendriksen PV, Wiik K, Lein HL. Thermal expansion and electrical conductivity of Fe and Cu doped MnCo2O4 spinel. Solid State Ionics 2018;326:90–9.
[9] Grolig JG, Froitzheim J, Svensson JE. Coated stainless steel 441 as interconnect material for solid oxide fuel cells: evolution of electrical properties. J Power Sources 2015;284:321–7.
[10] Falk-Windisch H, Claquesin J, Sattari M, Svensson JE, Froitzheim J. Co- and Ce/Co-coated ferritic stainless steel as interconnect material for intermediate temperature solid oxide fuel cells. J Power Sources 2017;343:1–10.
[11] Goebel C, et al. Long-term (4 year) degradation behavior of coated stainless steel 441 used for solid oxide fuel cell interconnect applications. J Power Sources 2020;449.
[12] Froitzheim J, et al. Long term study of Cr evaporation and high temperature corrosion behaviour of Co coated ferritic steel for solid oxide fuel cell interconnects. J Power Sources 2012;220:217–27.
[13] Qu W, Jian L, Ivey DG, Hill JM. Yttrium, cobalt and yttrium/cobalt oxide coatings on ferritic stainless steels for SOFC interconnects. J Power Sources 2006;157:335–50.
[14] Canovic S, et al. Oxidation of Co- and Ce-nanocoated FeCr steels: a microstructural investigation. Surf Coating Technol 2013;215:62–74.
[15] Fontana S, Chevalier S, Caboche G. Metallic interconnects for solid oxide fuel cell: performance of reactive element oxide coating during long time exposure. Mater Corros 2011;62:650–8.
[16] Zhao Q, Geng S, Chen G, Wang F. Application of sputtered NiFe2 alloy coating for SOFC interconnect steel. J Alloys Compd 2018;769:120–9.
[17] Jia C, et al. High temperature oxidation behavior of SUS430 SOFC interconnects with Mn-Co spinel coating in air. J Alloys Compd 2019;787:1327–35.
[18] Brylewski T, et al. Influence of Gd deposition on the oxidation behavior and electrical properties of a layered system consisting of Crofer 22 APU and MnCo2O4 spinel. Int J Hydrogen Energy 2021;46:6775–91.
[19] Lee S-I, et al. Highly dense Mn-Co spinel coating for protection of metallic interconnect of solid oxide fuel cells. J Electrochem Soc 2014;161:F1389–94.
[20] Irankhah R, Raissi B, Maghsoudipour A, Irankhah A, Ghashghai S. NiFe2O4 spinel protection coating for high-temperature solid oxide fuel cell interconnect application. J Mater Eng Perform 2016;25:1515–25.
[21] Zanchi E, et al. Iron doped manganese cobaltite spinel coatings produced by electrophoretic co-deposition on interconnects for solid oxide cells: microstructural and electrical characterization. J Power Sources 2020;455.
[22] Talic B, Molin S, Hendriksen PV, Lein HL. Effect of pre-oxidation on the oxidation resistance of Crofer 22 APU. Corrosion Sci 2018;138:189–99.
[23] Spotorno R, et al. Microstructural and electrical characterization of plasma sprayed Cu-Mn oxide spinels as coating on metallic interconnects for stacking solid oxide fuel cells. Fuel Cell 2015;15:728–34.
[24] Bianco M, et al. In-situ experimental benchmarking of solid oxide fuel cell metal interconnect solutions. J Power Sources 2020;461:228163.
[25] Grünwald N, et al. Microstructure and phase evolution of atmospheric plasma sprayed Mn-Co-Fe oxide protection layers for solid oxide fuel cells. J Eur Ceram Soc 2019;39:449–60.
[26] Bernuy-Lopez C, Bexell U, Stenstrom M, Norrby N, Westlinder. J. The time for industrialization has come: a pre-coated solution for the GW scale. ECS Trans 2021;103:1803–8.
[27] Falk-Windisch H, Sattari M, Svensson JE, Froitzheim J. Chromium vaporization from mechanically deformed pre-coated interconnects in Solid Oxide Fuel Cells. J Power Sources 2015;297:217–23.
[28] Magrasó A, Falk-Windisch H, Froitzheim J, Svensson JE, Haugsrud R. Reduced long term electrical resistance in Ce/Co-coated ferritic stainless steel for solid oxide fuel cell metallic interconnects. Int J Hydrogen Energy 2015;40:8579–85.
[29] Grolig JG, Froitzheim J, Svensson JE. Coated stainless steel 441 as interconnect material for solid oxide fuel cells: oxidation performance and chromium evaporation. J Power Sources 2014;248:1007–13.
[30] Talic B, Venkatachalam V, Hendriksen PV, Kiebach R. Comparison of MnCo2O4 coated Crofer 22 H, 441, 430 as interconnects for intermediate-temperature solid oxide fuel cell stacks. J Alloys Compd 2020;821:153229.
[31] Jablonski PD, Cowen CJ, Sears JS. Exploration of alloy 441 chemistry for solid oxide fuel cell interconnect application. J Power Sources 2010;195:813–20.
[32] Piccardo P, et al. K44M ferritic stainless steel as possible interconnect material for SOFC stack operating at 600 °c: characterization of the oxidation behaviour at early working stages. Int J Hydrogen Energy 2015;40:3726–38.
[33] Bongiorno V, Piccardo P, Anelli S, Spotorno R. Influence of surface finishing on high-temperature oxidation of AISI type 444 ferritic stainless steel used in SOFC stacks. Acta Metall. Sin. (English Lett. 2017;30:697–711.
[34] Da Conceição L, Dessemond L, Djurado E, Souza MMVM. Thin films of La0.7Sr0.3MnO3-δ dip-coated on Fe-Cr alloys for SOFC metallic interconnect. Int J Hydrogen Energy 2013;38:15335–47.
[35] Acchar W, et al. LaCrO3 composite coatings for AISI 444 stainless steel solid oxide fuel cell interconnects. Mater Res 2012;15:1064–9. scielo.
[36] Kim SH, Jun JH, Kim DH, Jun JH. Evaluation of STS 430 and STS 444 for SOFC interconnect applications. Corros. Sci. Technol. 2007;6:1–6.
[37] You PF, Zhang X, Zhang HL, Liu HJ, Zeng CL. Effect of CeO2 on oxidation and electrical behaviors of ferritic stainless steel interconnects with Ni–Fe coatings. Int J Hydrogen Energy 2018;43:7492–500.
[38] Choudhury A, Chandra H, Arora A. Application of solid oxide fuel cell technology for power generation - a review. Renew Sustain Energy Rev 2013;20:430–42.
[39] Zhao Q, Geng S, Chen G, Wang F. Initial oxidation behavior of ferritic stainless steel interconnect with sputtered NiFe2 alloy coating. Oxid Metals 2020;93:283–99.
[40] Reddy MJ, Svensson J-E, Froitzheim J. Reevaluating the Cr evaporation characteristics of Ce/Co coatings for interconnect applications. ECS Trans 2021;103:1899–905.

Please cite this article as: Reddy MJ et al., 11–23% Cr steels for solid oxide fuel cell interconnect applications at 800 °C – How the coating determines oxidation kinetics, International Journal of Hydrogen Energy, https://doi.org/10.1016/j.ijhydene.2022.11.326

[41] Froitzheim J, Ravash H, Larsson E, Johansson LG, Svensson JE. Investigation of chromium volatilization from FeCr interconnects by a denuder technique. J Electrochem Soc 2010;157:B1295.
[42] Falk Windisch H, Svensson J-E, Froitzheim J. Metallic thin-film Co- and Ce/Co-coated steels as interconnect material in IT-SOFC. ECS Trans 2017;78:1607–14.
[43] Goebel C, et al. Long term (4 Years) performance of Co/Ce coated 441 for SOFC interconnect applications. ECS Trans 2017;78:1675–9.
[44] Sachitanand R, Svensson JE, Froitzheim J. The influence of Cr evaporation on long term Cr depletion rates in ferritic stainless steels. Oxid Metals 2015;84:241–57.
[45] Tomas M, Goebel C, Svensson J-E, Froitzheim J. Cu-based coatings for IT-SOFC applications. ECS Trans 2019;91:2291–8.
[46] Reddy M, Froitzheim J. Report on chemical stability of the coated interconnects. 2020.
[47] Konysheva E, Seeling U, Besmehn A, Singheiser L, Hilpert K. Chromium vaporization of the ferritic steel Crofer22APU and ODS Cr5Fe1Y2O3 alloy. J Mater Sci 2007;42:5778–84.
[48] Ali-Löytty H, et al. The role of (FeCrSi)2(MoNb)-type Laves phase on the formation of Mn-rich protective oxide scale on ferritic stainless steel. Corrosion Sci 2018;132:214–22.
[49] Falk-Windisch H, Svensson JE, Froitzheim J. The effect of temperature on chromium vaporization and oxide scale growth on interconnect steels for Solid Oxide Fuel Cells. J Power Sources 2015;287:25–35.
[50] Reddy MJ, Svensson JE, Froitzheim J. Evaluating candidate materials for balance of plant components in SOFC: oxidation and Cr evaporation properties. Corrosion Sci 2021;109671. https://doi.org/10.1016/J.CORSCI.2021.109671.
[51] Harthøj A, Holt T, Møller P. Oxidation behaviour and electrical properties of cobalt/cerium oxide composite coatings for solid oxide fuel cell interconnects. J Power Sources 2015;281:227–37.
[52] Skilbred AWB, Haugsrud R. The effect of water vapour on the corrosion of Sandvik Sanergy HT under dual atmosphere conditions. Oxid Metals 2013;79:639–54.
[53] Trebbels R, Markus T, Singheiser L. Investigation of chromium vaporization from interconnector steels with spinel coatings. J Electrochem Soc 2010;157:B490.
[54] Collins C, et al. Chromium volatility of coated and uncoated steel interconnects for SOFCs. Surf Coating Technol 2006;201:4467–70.
[55] Kurokawa H, Jacobson CP, DeJonghe LC, Visco SJ. Chromium vaporization of bare and of coated iron-chromium alloys at 1073 K. Solid State Ionics 2007;178:287–96.
[56] Shu J, Bi H, Li X, Xu Z. The effects of molybdenum addition on high temperature oxidation behavior at 1,000 °c of type 444 ferritic stainless steel. Oxid Metals 2012;78:253–67.
[57] Faivre L, Santacreu PO, Acher A. A new ferritic stainless steel with improved thermo-mechanical fatigue resistance for exhaust parts30. Taylor & Francis; 2013. p. 36–42.
[58] Quadakkers WJ, Holzbrecher H, Briefs KG, Beske H. Differences in growth mechanisms of oxide scales formed on ODS and conventional wrought alloys. Oxid Metals 1989;32:67–88.
[59] Pint, B. A. Progress in understanding the reactive element effect since the whittle and stringer literature review.
[60] Chevalier S, Bonnet G, Borchardt G, Colson JC, Larpin JP. Mechanisms involved by reactive elements upon high temperature chromia scale growth. Mater Sci Forum 2001;369–372:327–36.
[61] Chevalier S, Valot C, Bonnet G, Colson JC, Larpin JP. The reactive element effect on thermally grown chromia scale residual stress. Mater Sci Eng, A 2003;343:257–64.
[62] Liu H, Stack MM, Lyon SB. Reactive element effects on the ionic transport processes in Cr2O3 scales. Solid State Ionics 1998;109:247–57.
[63] Toscan F, Antoni L, Wouters Y, Dupeux M, Galerie A. Oxidation kinetics and scale spallation of iron-chromium alloys with different titanium contents. In: Materials science forum, vols. 461–464. Trans Tech Publications Ltd; 2004. p. 705–12.
[64] Seo HS, Yun DW, Kim KY. Effect of Ti addition on the electric and ionic property of the oxide scale formed on the ferritic stainless steel for SOFC interconnect. Int J Hydrogen Energy 2012;37:16151–60.
[65] Froitzheim J, et al. Development of high strength ferritic steel for interconnect application in SOFCs. J Power Sources 2008;178:163–73.
[66] Juuti T, Karjalainen P, Rovatti L, Heikkinen E-P, Pohjanne P. Contribution of Mo and Si to laves-phase precipitation in type 444 steel and its effect on steel properties-VTT's Research Information Portal. In: 7th European stainless steel conference - science and market, como, Italy 21 - 23.9.2011. Associazione Italiana di Metallurgia AIM; 2011.
[67] Yang Z, et al. Investigation of iron-chromium-niobium-titanium ferritic stainless steel for solid oxide fuel cell interconnect applications. J Power Sources 2008;183:660–7.
[68] Fontana S, Chevalier S, Caboche G. Metallic interconnects for solid oxide fuel cell: performance of reactive element oxide coating during 10, 20 and 30 months exposure. Oxid Metals 2012;78:307–28.
[69] Fontana S, et al. Metallic interconnects for SOFC: characterisation of corrosion resistance and conductivity evaluation at operating temperature of differently coated alloys. J Power Sources 2007;171:652–62.
[70] Alman DE, Jablonski PD. Effect of minor elements and a Ce surface treatment on the oxidation behavior of an Fe-22Cr-0.5Mn (Crofer 22 APU) ferritic stainless steel. Int J Hydrogen Energy 2007;32:3743–53.
[71] Reddy MJ. Metallic materials in solid oxide fuel cells: oxidation and chromium evaporation properties. Chalmers University of Technology; 2021.
[72] Huczkowski P, et al. Oxidation limited life times of chromia forming ferritic steels. Mater Corros 2004;55:825–30.
[73] Stevenson JW, Yang ZG, Xia GG, Nie Z, Templeton JD. Long-term oxidation behavior of spinel-coated ferritic stainless steel for solid oxide fuel cell interconnect applications. J Power Sources 2013;231:256–63.
[74] Kingery WD, Bowen HK, Uhlmann DR. Introduction to ceramics. 2nd ed. 1976.
[75] Petric A, Ling H. Electrical conductivity and thermal expansion of spinels at elevated temperatures. J Am Ceram Soc 2007;90:1515–20.
[76] Holt A, Kofstad P. Electrical conductivity and defect structure of Cr2O3. II. Reduced temperatures (<~1000°C). Solid State Ionics 1994;69:137–43.
[77] Crawford JA, Vest RW. Electrical conductivity of single-crystal Cr2O3. J Appl Phys 1964;35:2413–8.
[78] Jo KH, Kim JH, Kim KM, Lee IS, Kim SJ. Development of a new cost effective Fe-Cr ferritic stainless steel for SOFC interconnect. Int J Hydrogen Energy 2015;40:9523–9.
[79] Huczkowski P, et al. Growth mechanisms and electrical conductivity of oxide scales on ferritic steels proposed as interconnect materials for SOFC's. Fuel Cell 2006;6:93–9.
[80] Mikkelsen L, Linderoth S, Bilde-Sørensen JB. The effect of silicon addition on the high temperature oxidation of a Fe-Cr alloy. In: Materials science forum, vols. 461–464. Trans Tech Publications Ltd; 2004. p. 117–22.
[81] Douglass DL, Armijo JS. The influence of manganese and silicon on the oxidation behavior of Co-20Cr. Oxid Metals 1971;3:185–202.

Please cite this article as: Reddy MJ et al., 11–23% Cr steels for solid oxide fuel cell interconnect applications at 800 °C – How the coating determines oxidation kinetics, International Journal of Hydrogen Energy, https://doi.org/10.1016/j.ijhydene.2022.11.326